Journal of Colloid and Interface Science **221,** 87–103 (2000)
Article ID jcis.1999.6563, available online at http://www.idealibrary.com on IDEAL®

# Aggregation of Charged Particles under Electrophoresis or Gravity at Arbitrary Péclet Numbers

Helen J. Wilson, Lorraine A. Pietraszewski, and Robert H. Davis[1]

*Department of Chemical Engineering, University of Colorado, Boulder, Colorado 80309-0424*

Received May 25, 1999; accepted September 30, 1999

**Collision efficiencies are considered for colloidal suspensions of solid spheres moving in a viscous fluid under the influence of electrophoresis or gravity, Brownian motion, and electrostatic and van der Waals forces. The results are compared to those for convection (electrophoresis or gravity) and diffusion (Brownian motion) acting independently. The collision efficiency increases by many orders of magnitude over that predicted by simply adding diffusive and convective efficiencies in a specific parameter regime. This regime occurs when there is a large energy barrier in the interparticle potential, causing a stable region of parameter space if there is no diffusion. Brownian motion alone will only cause small amounts of aggregation under these conditions. However, for electric fields or buoyancy effects which are only slightly too weak to allow particles to overcome the potential barrier, the addition of weak Brownian motion to a system with convection can cause significant numbers of particles to overcome the energy barrier and aggregate.** 

*Key Words:* **aggregation; Brownian motion; collision efficiency; electrophoresis; gravity.**

## 1. INTRODUCTION

The analysis of suspensions of small particles is of interest in both industry and nature. Water and wastewater treatment plants require knowledge of the fate of small particles in their systems. Drug delivery utilizing small particulates, such as encapsulation or adhesion to fines, requires knowledge of the behavior of particles in both production and utilization. Silting processes in rivers are driven by sedimentation of small particles.

When an electric field is applied to a solution containing charged particles, the particles will migrate through the solution by *electrophoresis*. This phenomenon is used, for example, in the separation of different types of particles in biological applications. In a suspension of particles which are not neutrally buoyant, the particles will sediment under gravity. In these processes, it may be either desirable or undesirable for the particles to flocculate or aggregate during migration. Because of the industrial relevance of the processes involved, as well as for the fundamental underlying science, the study of aggregation rates for charged particles undergoing electrophoresis or sedimentation is of interest.

Much of the fundamental basis of this subject has been laid out by Smoluchowski (1), and Russel *et al*. (2) have provided a thorough reference text to which we refer throughout this paper. Relevant early work includes the standard form of interparticle potentials, which is developed from DLVO theory (Derjaguin and Landau (3) and Verwey and Overbeek (4)), which assumes that the net interparticle potential is the sum of the attractive and repulsive potentials, and the basic form of the attractive van der Waals potential (Hamaker (5)).

Theoretical studies of aggregation have been carried out in the past. In 1970, the rate of aggregation for a purely Brownian suspension with an arbitrary interparticle force was calculated by Spielman (6), and an asymptotic calculation for Brownian particles with weak gravitational motion was carried out by Melik and Fogler in 1984 (7). For negligible Brownian motion, a trajectory analysis method may be used. For a gravitational driving force, Melik and Fogler (7) and Davis (8), also in 1984, used trajectory analyses to predict collision rates; however, the hydrodynamic resistance and mobility functions for electrophoresis were not calculated until much later, so the analysis of electrophoretic motion lagged by several years. In 1995, Nichols *et al*. (9) considered aggregation due to either gravitational or electrophoretic motion. The same method was used by Wang *et al*. (10) to investigate the effect of simultaneous gravitational and electrophoretic driving forces on the aggregation rate. In 1999, Zeng *et al*. (11) produced a bispherical-coodinates method of calculating the electrophoretic hydrodynamic mobility functions, so that these mobilities are now as freely available as the gravitational mobilities.

The addition of Brownian motion to a system with electrophoresis or gravity makes a trajectory analysis impossible, and only recently have numerical techniques been devised which can deal satisfactorily with moderate (neither asymptotically large nor small) Brownian motion. In 1994, Zinchenko and Davis (12) devised a novel numerical technique for studying aggregation rates of drops at arbitrary Péclet numbers (where the Péclet number is a measure of the driving velocities relative to Brownian motion) and applied it to the gravity-induced coalescence of fluid drops in an emulsion. In that case, the drops

[1] To whom correspondence should be addressed. E-mail: Robert.Davis@colorado.edu.



0021-9797/00 $35.00

were not charged, so there was van der Waals attraction but no electrostatic force. In 1995, the same authors extended their method to the more challenging problem of aggregation driven by a shear flow (13). As far as we know, however, no related work has yet been performed for charged particles at arbitrary Péclet numbers when electrostatic interparticle forces are important.

## 2. FORMULATION OF THE PROBLEM

Consider a dilute, locally homogeneous suspension containing electrically charged, solid spherical particles dispersed in a viscous Newtonian fluid. We examine two distinct possibilities for the system. In the *electrophoresis* scenario, the particles are neutrally buoyant and the whole system is placed in an electric field, so that an isolated particle has a constant velocity due to electrophoresis, proportional to its surface charge and to the applied electric field. In the alternative, *gravity* scenario, there is no applied electric field and the particles all have the same density, which is different from that of the ambient fluid. In both cases, the system is assumed to be isothermal, and the particles are sufficiently small that their inertia may be neglected and the quasi-steady Stokes equations hold in the surrounding fluid.

For dilute suspensions, the probability of a third particle influencing the relative motion of two interacting particles is small, so the analysis is restricted to binary interactions of particles with radii $a_1$ and $a_2$, as shown in Fig. 1. The motion of the particles is affected by Brownian motion, by electrostatic forces caused by the interaction of their electrical double layers, by the particles' individual electrophoretic or gravitational velocities, and by attractive interparticle van der Waals forces. In the electrophoretic case, motion due to gravity may be neglected as the particles are either neutrally buoyant or very small.

In the dilute limit, the pair distribution funciton $p(\boldsymbol{r})$, which is the probability density of finding a sphere of radius $a_1$ centered at $\boldsymbol{r}$ given that there is a sphere of radius $a_2$ centered at the origin, satisfies the quasi-steady Fokker–Planck equation:

$$\boldsymbol{\nabla} \cdot [p(\boldsymbol{r})\boldsymbol{V}_{12}(\boldsymbol{r})] = 0. \qquad [1]$$

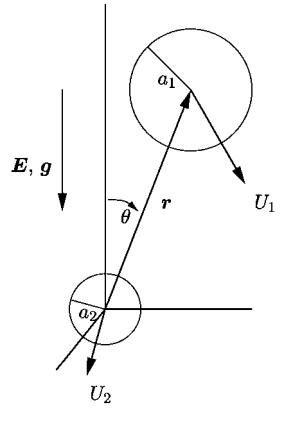


**FIG. 1.** Schematic representation of the coordinate system used for the relative motion of two different-sized particles.

Here, $\boldsymbol{V}_{12}$ is of the form (14, 15)

$$\begin{aligned}\boldsymbol{V}_{12}(\boldsymbol{r}) = \boldsymbol{V}_{12}^{(0)} \cdot [\boldsymbol{nn}L(s) + (\boldsymbol{I} - \boldsymbol{nn})M(s)] \\ - \frac{D_{12}^{(0)}}{kT}[\boldsymbol{nn}G(s) + (\boldsymbol{I} - \boldsymbol{nn})H(s)] \cdot \boldsymbol{\nabla}\Phi_{12} \\ - D_{12}^{(0)}[\boldsymbol{nn}G(s) + (\boldsymbol{I} - \boldsymbol{nn})H(s)] \cdot \boldsymbol{\nabla}(\ln p(\boldsymbol{r})), \quad [2]\end{aligned}$$

where $L$, $M$, $G$, and $H$ are hydrodynamic relative mobility functions, $s = r/a$, where $a = (a_1 + a_2)/2$ is the average of the particle radii, $\boldsymbol{n} = \boldsymbol{r}/r$, $\boldsymbol{I}$ is the unit second-order tensor, and $\Phi_{12}$ is the interparticle potential. This potential describes the interparticle forces for both van der Waals and electrostatic interactions. The gravitational mobility functions are discussed by Zinchenko and Davis (12), and the electrophoretic mobilities by Zeng *et al.* (11). We do not elaborate further here on their form. The method used to calculate the mobility functions for electrophoresis depends on the condition $\kappa a \gg 1$, where $\kappa^{-1}$ is the double-layer thickness.

$\boldsymbol{V}_{12}^{(0)}$ is the relative velocity due to either gravity or electrophoresis, given by the difference between the velocities each sphere would experience in isolation (1),

$$\boldsymbol{V}_{12}^{(E;0)} = \frac{\epsilon(\zeta_1 - \zeta_2)\boldsymbol{E}}{\mu}, \qquad [3]$$

$$\boldsymbol{V}_{12}^{(G;0)} = \frac{2\Delta\rho(1 - \lambda^2)a_1^2\boldsymbol{g}}{9\mu}, \qquad [4]$$

where $\zeta_i$ is the charge on particle $i$, $\lambda$ is the radius ratio $a_2/a_1$, $\boldsymbol{E}$ is the imposed electric field and $\boldsymbol{g}$ the gravitational field, the fluid has viscosity $\mu$ and permittivity $\epsilon$, and $\Delta\rho$ is the density difference between the particles and the fluid. $D_{12}^{(0)}$ is the relative diffusivity due to Brownian motion for two widely separated particles,

$$D_{12}^{(0)} = \frac{(a_1 + a_2)kT}{6\pi\mu a_1 a_2}, \qquad [5]$$

where $k$ is the Boltzmann constant and $T$ the absolute temperature. The boundary conditions are (12)

$$p = 0 \quad \text{for } r = a_1 + a_2, \qquad [6]$$

$$p \to 1 \quad \text{as } r \to \infty. \qquad [7]$$

The former of these may be taken to indicate that once a pair of particles has made contact, a permanent doublet is formed and the particles are no longer free to separate (for a justification, see, for example, Davis (8)).

We define the collision rate $J_{12}$ as the flux of pairs into the collision surface $r = a_1 + a_2$,

$$J_{12} = -n_1 n_2 \int_{r \to a_1 + a_2} p\boldsymbol{V}_{12} \cdot \boldsymbol{n}\, \mathrm{d}A, \qquad [8]$$

where $n_1$, $n_2$ are the number densities of particles of types 1 and 2, respectively. In the "Smoluchowski limit" when the particles move under electrophoresis or gravity alone, with no Brownian motion, interparticle forces, or hydrodynamic interactions, the collision rate is

$$J_{12}^{(0)} = n_1 n_2 V_{12}^{(0)} \pi (a_1 + a_2)^2, \qquad [9]$$

and we define the collision efficiency $E_{12}$ to be the ratio of the actual collision rate to this idealized rate:

$$E_{12} = J_{12} \big/ J_{12}^{(0)}. \qquad [10]$$

## 3. THE PROBLEM IN DIMENSIONLESS FORM

We define the dimensionless parameters

$$\begin{aligned}
\lambda &= a_2/a_1, \\
\beta &= \zeta_2/\zeta_1, \\
N_{\mathrm{R}} &= \epsilon \zeta_1 \zeta_2 a/A, \\
Q_{\mathrm{E}} &= 12\pi\epsilon\zeta_1|(1-\beta)|Ea^2\lambda/A(1+\lambda)^2, \\
Q_{\mathrm{G}} &= 2\pi a_1^4(1-\lambda^2)\lambda\Delta\rho g/3A, \\
\hat{A} &= A/kT, \\
\nu &= \lambda_{\mathrm{L}}/a, \text{ and } \kappa a,
\end{aligned}$$

where $A$ is the Hamaker constant, $\lambda_{\mathrm{L}}$ is the London wavelength (taken as 0.1 $\mu$m), $\kappa^{-1}$ is the Debye length, $\lambda$ is the size ratio between the two particles, and $\beta$ is the ratio of their surface charges. We label the particles so that $a_2 \le a_1$ i.e., $0 < \lambda \le 1$. $N_{\mathrm{R}}$ is a measure of the strength of the (usually repulsive) electrostatic force acting between them (relative to the attractive van der Waals force). Note that $N_{\mathrm{R}}$ as it is defined here is different from the $N_{\mathrm{R}}$ of Nichols *et al.* (9) by a factor of $\beta$. We made this choice to emphasize the symmetry of the problem to the labels on each particle. $Q_{\mathrm{E}}$ and $Q_{\mathrm{G}}$ measure the strength of the electrophoretic or gravitational relative velocity (as it would be in the absence of hydrodynamical interactions) compared to that due to the attractive van der Waals forces, and $\hat{A}$ measures the strength of the interparticle potential relative to Brownian motion. The parameter $\kappa a$ is small when the electrical double layer between the particles is large, and vice versa, and it is dependent on the ionic strength. Finally, $\nu$ is the retardation parameter, which modifies the van der Waals force.

The relative mobility functions for motion along the line of centers ($L$ and $G$) and motion normal to the line of centers ($M$ and $H$) describe the effects of hydrodynamic interactions between the two particles. On the assumption that $\kappa a \gg 1$, they depend only on the size ratio $\lambda$ and the interparticle separation $s$. They are invariant to particle labels, so $L(s, \lambda) = L(s, \lambda^{-1})$ and similar relations are true for $G$, $H$, and $M$.

Assuming that the interparticle force acts along the line of centers, we have (from Eq. [2]) the expression for the dimensionless relative velocity, $\boldsymbol{u} = \boldsymbol{V}_{12}/V_{12}^{(0)}$,

$$\begin{aligned}
u = &-L(s)\cos\theta \boldsymbol{e}_r + M(s)\sin\theta \boldsymbol{e}_\theta - \frac{1}{Q_{(\mathrm{G,E})}} G(s)\phi'(s)\boldsymbol{e}_r \\
&- \frac{1}{\hat{A}Q_{(\mathrm{G,E})}}\left[ G(s)\frac{\partial(\ln p)}{\partial s}\boldsymbol{e}_r + \frac{H(s)}{s}\frac{\partial(\ln p)}{\partial\theta}\boldsymbol{e}_\theta \right], \qquad [11]
\end{aligned}$$

where $\phi = \Phi_{12}/A$ is the dimensionless interparticle potential, $\phi' = \mathrm{d}\phi/\mathrm{d}s$, and $\boldsymbol{e}_r$ and $\boldsymbol{e}_\theta$ are unit vectors in the radial and tangential directions, respectively, of the spherical coordinate system shown in Fig. 1.

For simpler comparison with the methods and results of (12), we also define the Péclet number $\mathrm{Pe} = aV_{12}^{(0)}/D_{12}^{(0)} = \hat{A}Q_{(\mathrm{G,E})}$. Since, in most physical situations, $\hat{A} \sim O(1)$, the quantity $Q_{(\mathrm{G,E})}$ has the same physical effect as the Péclet number.

### 3.1. Brownian Motion Alone

For pure Brownian motion, the collision rate $J_{12}$ is given by (see, for example, Russel *et al.* (2))

$$J_{12} = 4\pi n_1 n_2 D_{12}^{(0)} \left/ \left( \int_{a_1+a_2}^{\infty} \frac{\exp(\Phi_{12}/kT)}{r^2 G}\,\mathrm{d}r \right). \right. \qquad [12]$$

This expression yields a collision efficiency for Brownian motion alone of

$$E_{12} = \frac{C}{\hat{A}Q_{(\mathrm{G,E})}} = C\mathrm{Pe}^{-1}, \qquad [13]$$

in which

$$C = \left[ \int_2^{\infty} \frac{\exp(\hat{A}\phi(s))}{s^2 G}\,\mathrm{d}s \right]^{-1}. \qquad [14]$$

We note that, although the collision rate $J_{12}$ does not depend on the Péclet number, the gravitational or electrophoretic Smoluchowski limit, $J_{12}^{(0)}$, does depend on $V_{12}^{(0)}$, and hence on Pe, and this is why the Brownian collision efficiency has a dependency on the Péclet number.

It has been shown by Melik and Fogler (7) for weak gravitational motion, and the result is true equally for weak electrophoresis, that the two-term asymptotics for small Pe are

$$E_{12} \sim \frac{C}{\mathrm{Pe}} + \frac{C^2}{2}, \qquad [15]$$

but the pure Brownian result is given by the first term alone.

In this paper, we use numerical quadrature to calculate $C$ and use it as a check on the small Péclet number limit of the more intricate code used for finite Péclet numbers.

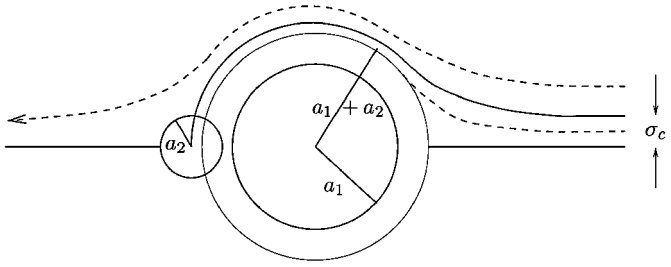


**FIG. 2.** Schematic diagram showing the critical trajectory dividing aggregation from escape, and the offset $\sigma_c$ which can be used to define the collision efficiency.

### 3.2. Electrophoresis or Gravity Alone

In the case in which there is no Brownian motion, the collision efficiency may be calculated using trajectory methods (as used, for example, by Nichols *et al*. (9)). The core of the method is an integration backward along the limiting trajectory which separates capture (or aggregation) and escape. This trajectory is found at the rear of sphere 1, at the point where $\boldsymbol{u}$ vanishes. Then it is integrated upstream to find its offset at infinity, $\sigma_c$ (shown in Fig. 2). The collision efficiency may then be expressed as

$$E_{12} = \frac{\pi\sigma_c^2}{\pi(a_1+a_2)^2} = \left(\frac{\sigma_c}{a_1+a_2}\right)^2. \qquad [16]$$

When both Brownian motion and either electrophoresis or gravity (which we will refer to collectively as "convection") act, but the Brownian motion is weak compared to the convection (i.e., at high Péclet numbers), the collision efficiency should be very close to that predicted for convection acting alone, and this serves as a further check on our results.

In addition, for a case in which the electrostatic force is absent, Davis (8) has calculated an asymptotic form for the collision efficiency due to gravity with weak Brownian motion,

$$E_{12} \sim \frac{\alpha}{Q^\beta}, \qquad [17]$$

in which $\alpha$ and $\beta$ are constant to leading order at $Q \gg 1$. In calculating this (simplified) form, logarithmic terms in the near-field of the mobility function $M$ were neglected; in electrophoresis, there are no such terms, so the asymptotic form is valid for a wider range of $Q$.

### 3.3. Interparticle Potential

In this section was specify the form of $\phi'$, the derivative of the interparticle potential, as this term is used in Eq. [11]. The attractive force occurs due to London–van der Waals attraction, attributed to electromagnetic and magnetic molecular polarizations producing a fluctuating electromagnetic field.

Traditionally the form suggested by Hamaker (5) has been used for this attractive force. However, this form usually overpredicts the attraction (Elimelech *et al*. (16)). Retardation effects arise due to the time dependence of electromagnetic propagation, which effectively reduces the amount of interaction and corrects the overestimation. In some circumstances, the inclusion of retardation effects can modify the collision rate by a factor of two or more (see, for example, Fig. 7 of (8)). We adopt, following Zinchenko and Davis (12), the Ho and Higuchi (17) approximation in the near-field regioin $s - 2 \ll 1$:

$$\phi'_{\mathrm{vdW}}(s) = \frac{\lambda}{(1+\lambda)^2}\frac{0.06\nu(s-2+0.045\nu)}{(s-2)^2(s-2+0.09\nu)^2}. \qquad [18]$$

The derivation of the form used in the large region $s - 2 > 0.08\nu$ is given in Appendix D of Zinchenko and Davis (12) and is not reproduced here. The primary result is

$$\phi'_{\mathrm{vdW}}(s) = \frac{\alpha_1+\alpha_2}{120}\left[2.45\Omega(J_7+J_8) - \frac{2.17}{12}\Omega^2(J_8+J_9) + \frac{0.59}{168}\Omega^3(J_9+J_{10})\right], \qquad [19]$$

in which $\Omega = \nu/(\pi s)$,

$$\alpha_1 = 2/(1+\lambda)s, \qquad [20]$$

$$\alpha_2 = 2\lambda/(1+\lambda)s, \qquad [21]$$

$$f_n(x) = (n-8)!/(1+x)^{n-7} \quad \text{for } n \geq 8, \qquad [22]$$

$$f_7(x) = -\ln(1+x), \qquad [23]$$

and

$$\begin{aligned} J_n = {} & f_n(\alpha_1+\alpha_2) + f_n(-\alpha_1-\alpha_2) - f_n(\alpha_2-\alpha_1) - f_n(\alpha_1-\alpha_2) \\ & + (n-6)!\left[\frac{\alpha_1\alpha_2}{(1-\alpha_1-\alpha_2)^{n-5}} + \frac{\alpha_1\alpha_2}{(1+\alpha_1+\alpha_2)^{n-5}} \right. \\ & \left. + \frac{\alpha_1\alpha_2}{(1+\alpha_1-\alpha_2)^{n-5}} + \frac{\alpha_1\alpha_2}{(1-\alpha_1+\alpha_2)^{n-5}}\right] \\ & + (n-7)!\left[\frac{\alpha_1-\alpha_2}{(1+\alpha_2-\alpha_1)^{n-6}} + \frac{\alpha_2-\alpha_1}{(1+\alpha_1-\alpha_2)^{n-6}} \right. \\ & \left. + \frac{\alpha_1+\alpha_2}{(1+\alpha_1+\alpha_2)^{n-6}} - \frac{\alpha_1+\alpha_2}{(1-\alpha_1-\alpha_2)^{n-6}}\right]. \end{aligned} \qquad [24]$$

The potential for electrostatic interaction is given, for $\kappa a \gg 1$, by Hogg *et al*. (19) as

$$\phi'_{\mathrm{Rep}}(s) = -N_{\mathrm{R}}\kappa a\frac{\lambda}{(1+\lambda)^2} \times\left[\frac{2e^{-\kappa a(s-2)} - (\beta+\beta^{-1})e^{-2\kappa a(s-2)}}{1-e^{-2\kappa a(s-2)}}\right]. \qquad [25]$$

In practice the errors in this approximation are not too large

provided $\kappa a \geq 5$ and $\zeta_i \leq 25$ mV (9). The potential given by Eq. [25] is generally repulsive ($\phi' < 0$) for particles with surface potentials of the same sign ($\beta > 0$), but it can be attractive at sufficiently small separations when $\beta \neq 1$ (9, 19). We are only considering the constant-potential regime here, and we will not consider the problems associated with double-layer relaxation rates (18).

## 4. NUMERICAL METHOD AND TESTS

The code for finite Péclet numbers was created from the parabolized code described in Zinchenko and Davis (12). The method consists of neglecting the angular derivatives in the Fokker–Planck equation, which produces a parabolic partial differential equation that is much easier to solve numerically than is the original form. Because the probability distribution is spherically symmetric at both high and low Péclet numbers, this approximation is relatively good over the full range of parameters. The equation is written as a system of two first-order equations and is discretized in the angular and radial directions for numerical solution. Two power expansions are derived, with successive terms calculated iteratively. Because the hydrodynamic resistance functions for two spheres are singular at close approach, the contact boundary condition is actually applied at a small distance from contact (typically around $10^{-3}$ radius). In effect, this means that if two particles come this close together they are assumed to aggregate. At moderate Péclet numbers we also show sample results from a much slower code which solves the full Fokker–Planck equation, to verify that the parabolic approximation is not producing misleading results. The code written by Zinchenko and Davis (12) deals with gravitational motion, so changes were made in order to allow selection of the definitions of the Péclet number and the hydrodynamic mobility functions appropriate for either gravity or electrophoresis, and to add an interparticle potential force which includes electrostatic interaction. A code to generate the electrophoretic mobility functions was provided by Zeng *et al*. (11). This section explains the methods used to check the modified code.

Nichols *et al*. (9) performed a trajectory analysis of the interaction between two non-Brownian spheres influenced by hydrodynamic forces, electrophoresis or gravity, retarded van der Waals attraction, and electrostatic repulsion. Our limiting case $\mathrm{Pe} \to \infty$ should be equivalent to their results. We have used a trajectory integration method similar to theirs, which includes only the effects of electrophoresis or gravity and the interparticle potential. In the special case $\lambda = 1$, the two spheres are the same size, so in (9) gravity has no effect. Our trajectory-method code for electrophoresis alone is therefore checked by reproduction of their Fig. 8, and since the only change we have made to our gravitational code is the addition of an electrostatic force, a test of the electrophoresis code is sufficient to prove the validity of both.

In the full code, we cannot fully attain the limit $\mathrm{Pe} \to \infty$, but we can consider a series of Péclet numbers tending to infinity. We choose a single point to check against a trajectory code and calculate using several values of Pe for a fixed value of $Q_\mathrm{E}$. We can then extrapolate to $\mathrm{Pe} = \infty$. Fixing $Q_\mathrm{E}$ while Pe becomes large is equivalent to letting $\hat{A} \to \infty$.

We choose to check the specific point $Q_\mathrm{E} = 1$, for which $\mathrm{Pe} = \hat{A}$, against the trajectory code. The results for finite Péclet numbers are shown in Fig. 3; the extrapolation to $\mathrm{Pe} = \infty$ from the last two points on the graph gives, for $\lambda = 1$, $E_{12} = 0.7185$, and for $\lambda = 0.5$, $E_{12} = 0.6611$, which compare favorably with the trajectory analysis results of $E_{12} = 0.7186$ and $E_{12} = 0.6611$, respectively. Thus, we have verification of our electrophoretic mobility functions and the electrostatic potential.

The bulk of the unchanged code for finite values of $\hat{A}$ was tested using the simple problem referred to by Zinchenko and Davis (12) as "the Smoluchowski model for finite Péclet number." This consists of neglecting hydrodynamic forces and interparticle forces and is expressed as $L = M = G = H = 1$ and $\phi' = 0$. The problem becomes independent of the particle size ratio $\lambda$. If we let the $z$-direction be parallel to driving field $\boldsymbol{E}$ or $\boldsymbol{g}$, the governing equations become

$$\boldsymbol{\nabla} \cdot (p\mathbf{u}) = 0, \qquad [26]$$

$$\mathbf{u} = -\cos\theta \boldsymbol{e}_r + \sin\theta \boldsymbol{e}_\theta - \frac{1}{\hat{A} Q_{(\mathrm{G,E})}} \left[ \frac{1}{p} \frac{\partial p}{\partial s} \boldsymbol{e}_r + \frac{1}{ps} \frac{\partial p}{\partial \theta} \boldsymbol{e}_\theta \right], \qquad [27]$$

which is equivalent to

$$\hat{A} Q_{(\mathrm{G,E})} \frac{\partial p}{\partial \hat{z}} - \nabla^2 p = 0. \qquad [28]$$

This equation has an analytical series solution, given in Appendix C of Zinchenko and Davis (12) by substituting $\mathrm{Pe} = \hat{A} Q_{(\mathrm{G,E})}$. Their sample analytical results (Table 1, p. 131 of (12)) and results from their parabolized code are compared to our numerical results in Table 1. The numerical parameters $I$ and $s_I$ are as defined in (12). Our errors (introduced by the parabolization approximation) are typically 1–4%, which is acceptable given the uncertainties in the interparticle potential and the parameters in any physical situation, and this result also serves as a check on our redefined Péclet number for electrophoresis.

It is interesting to note the behavior of this simple system for very low Péclet numbers. As discussed in (12), the two-term asymptotics for $\mathrm{Pe} \ll 1$ are

$$E_{12} \approx C\mathrm{Pe}^{-1} + \frac{1}{2} C^2, \qquad [29]$$

in which

$$C = \left( \int_2^\infty \frac{\mathrm{d}s}{s^2 G} \right). \qquad [30]$$

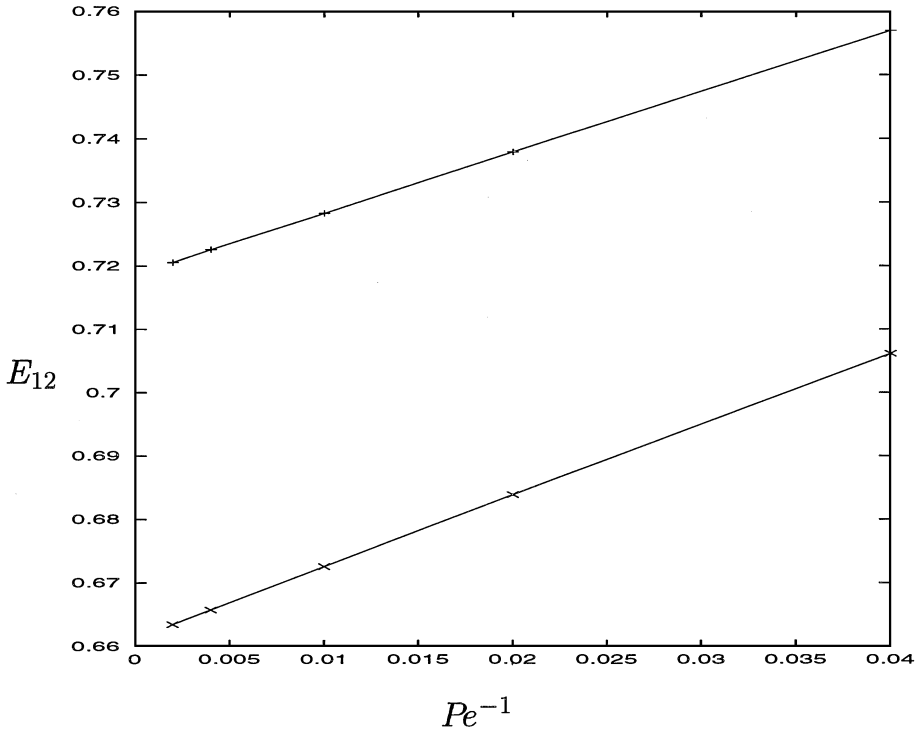


**FIG. 3.** Collision efficiencies for checking against a trajectory analysis. The parameter values are $\kappa a = 10^4$, $\beta = 0.5$, $N_R = 500$, $Q_E = 1$, $\nu = 0.033$ and $\lambda = 1$ (+) or $\lambda = 1/2$ (×). The trajectory analysis limit is given by Pe$\rightarrow \infty$.

Our calculations yield a value of $C = 1.998$, and thus the asymptotic form at a Péclet number of 0.03 gives $E_{12} \approx 68.60$. This result agrees closely with the analytical solution $E_{12} = 68.65$ from (12).

As an extra check on the validity of the parabolization approximation, we use an exact numerical solution of the full Fokker–Planck equation (also described in Zinchenko and Davis (12)). This code is far slower than the parabolized version and is therefore impractical for comprehensive calculations, but a few points have been calculated to demonstrate that the trends indicated by the approximate results are correct. These points have all been chosen to be at moderate Péclet numbers, because in the limit of high or low Péclet numbers the pair distribution function is spherically symmetrical, and the parabolized approximation becomes exact. Since the parabolization consists of neglecting axial derivatives, we expect the approximation to have the largest errors for moderate Pe.

## 5. RESULTS AND DISCUSSION

### 5.1. Form of the Potential

The behavior of the collision efficiency $E_{12}$ with varying driving force $Q_{(G,E)}$ depends critically on the form of the interparticle potential. A very thin double layer, with low zeta potential, produces a potential energy which is attractive for all separations, consisting of an infinitely deep (primary) well at very close separations. Thus, there is no energy barrier which protects against collision. Significantly decreasing the ionic strength, or slightly decreasing the ionic strength and increasing the zeta potential,

**TABLE 1**
**The Collision Efficiency for the Smoluchowski Model at Finite Péclet Numbers**

| Pe | 0.03 | 0.1 | 0.3 | 1 | 3 | 10 |
|---|---|---|---|---|---|---|
| Numerical solution | | | | | | |
| $s_I = 20$ | 74.42 | 23.11 | 8.8999 | 3.7958 | 2.1608 | 1.4730 |
| $s_I = 40$ | 70.99 | 22.69 | 8.8960 | 3.7958 | 2.1608 | 1.4730 |
| Extrapolation | | | | | | |
| $s_I = \infty$ | 67.56 | 22.27 | 8.8921 | 3.7958 | 2.1608 | 1.4730 |
| Analytical solution | 68.65 | 21.94 | 8.5121 | 3.6568 | 2.1170 | 1.4619 |
| Relative error | 1.6% | 1.5% | 4.4% | 3.8% | 2.0% | 0.8% |

*Note.* The results are all at $I = 4000$.

will produce a potential energy barrier inhibiting particles from entering into the primary well at very close separations. The far-field forms of the potentials guarantee that in this case there will also be an additional secondary minimum, at larger separations. A secondary minimum in the potential energy plot indicates the possibility of secondary aggregation of particles.

For collision (or primary aggregation) to occur with a double layer present, a particle must possess sufficient energy to overcome the barrier. Once the barrier is ascended, particles are held together by very strong van der Waals forces, and separation is extremely difficult. The secondary minimum in the potential energy curve is due to the functional dependence of the attractive and repulsive forces on the separation distance, and particles here are held in weak aggregates.

In summary, the potential can take two general shapes:

Type I—The potential is attractive for all values of the interparticle separation.

Type II—There is an energy barrier between the primary minimum (for particles coming into contact) and a weak secondary minimum, in which secondary aggregation is possible.

The parameter regimes in which each type of potential can occur are widely known and will not be repeated here.

### 5.2. *The Effect of Brownian Motion at Moderate Péclet Numbers*

Our first examples use a Type II potential with a varying repulsive barrier, since the synergistic effect in the absence of a repulsive barrier (Type I potential) is only modest and has been examined elsewhere (12). In these examples the secondary minimum is so distant and weak as to have no effect on the dynamics of the system, and the important part of the potential is the energy barrier. The parameters are $\kappa a = 10$, $\hat{A} = 1.25$, $\nu = 0.044$, and $N_R = 10$, 30, or 50. The dimensionless height of the potential barrier is, for gravity and electrophoresis, respectively, 2.223 and 2.040 for $N_R = 10$, 7.437 and 6.548 for $N_R = 30$, and 12.864 and 11.111 for $N_R = 50$. It may be seen that the barrier height is an approximately linear function of $N_R$ (in all these cases, the barrier height divided by $N_R$ is between 0.20 and 0.26). For electrophoresis, the particles are considered to be of equal size (so that there is no gravitational relative motion), and for gravity they have the same $\zeta$-potential, so that there is no electrophoretic relative motion. Therefore, the remaining parameters are, for gravity, $\lambda = 0.5$, $\beta = 1$, and for electrophoresis, $\lambda = 1$, $\beta = 0.5$. The collision efficiencies for diffusive, convective, and combined cases are shown in Figs. 4 (for electrophoresis) and 5 (for gravity). The collision efficiency due to the combined effects of

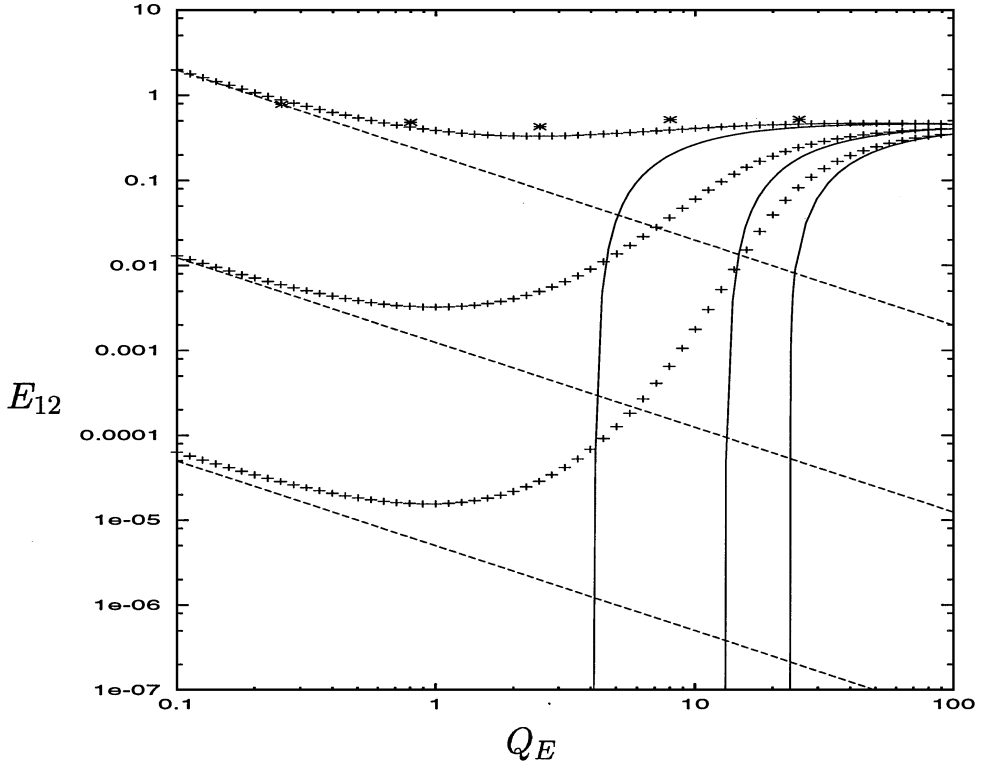


**FIG. 4.** The dramatic effect of adding Brownian motion in what would be a stable region of parameter space if Brownian motion effects were not taken into account. The parameter values are $\kappa a = 10$, $\beta = 0.5$, $\nu = 0.044$, and $\lambda = 1$ (electrophoresis only). The dashed lines are the pure Brownian case, and the solid curves the pure electrophoresis case. The plusses (+) indicate the same scenario with $\hat{A} = 1.25$. The three sets of curves are given by, reading from top to bottom, $N_R = 10$, $N_R = 30$, and $N_R = 50$. The extra points (∗) are from an exact calculation (i.e., without the parabolization approximation) and confirm that the errors inherent in the parabolization are not causing misleading results.

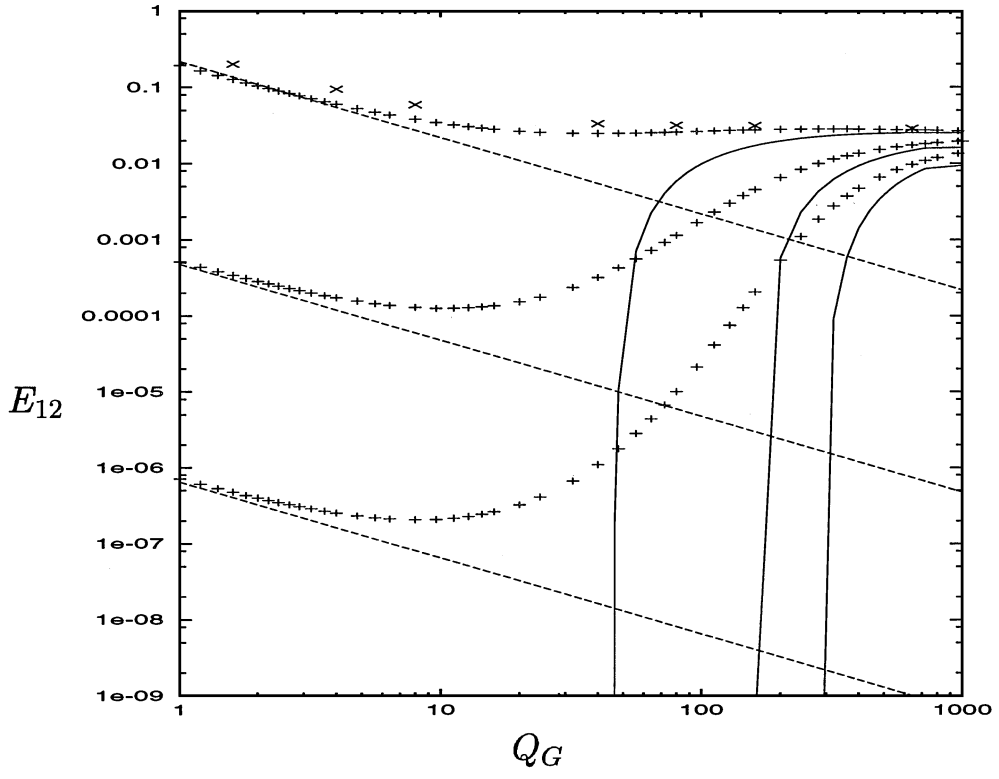


**FIG. 5.** The dramatic effect of adding Brownian motion in what would be a stable region of parameter space if only gravitational effects were taken into account. The parameter values are $\hat{A} = 1.25$, $\kappa a = 10$, $\lambda = 0.5$, $\nu = 0.044$, and $\beta = 1$ (gravity only). The dashed lines are the pure Brownian case, the solid lines are gravitational motion only, and the (+) are for the combined effects. The three sets of curves are given by, starting from the top, $N_R = 10$, $N_R = 30$, and $N_R = 50$. The maximum correction factor for $N_R = 10$ is $\approx 8$, for $N_R = 30$, $\approx 1500$, and for $N_R = 50$, $\approx 8000$. The points ($*$) above the graph were generated from the full (not the parabolized) calculation for gravity.

electrophoresis/gravity and diffusion is plotted in points. When the Péclet number is low (toward the left of the graph), the electrophoretic or gravitational motion has little effect and the collision efficiency is primarily due to Brownian motion; thus, the points tend toward the straight lines, which represent the collision efficiency due to diffusion acting alone. At high Péclet numbers (the right side of the graph), the reverse is true. The effect of diffusion is weak, and the actual collision efficiency is very close to that predicted (using a trajectory analysis) for the situation with no Brownian motion, which is plotted as a solid curve.

We define the *correction factor* to be, for a given set of parameters $\{\lambda, \beta, \kappa a, N_R, \nu, \hat{A}\}$, the ratio of the synergistic collision efficiency $E_{12}$ to that predicted by adding the independent Brownian and electrophoretic or gravitational contributions. Following this, the *maximum correction factor* (MCF) is the maximum of the correction factor over the full range of Péclet numbers. In a similar vein, we define the *absolute correction* to be the true collision efficiency minus that predicted by the additive approximation, and the *maximum absolute correction* (MAC) to be the maximum of this quantity over the range of Péclet numbers.

In these two figures, it is seen that the maximum correction factor increases with increasing $N_R$: for electrophoresis, the values are MCF $= 7.21$ at $N_R = 10$, MCF $= 1.02 \times 10^3$ at $N_R = 30$, and MCF $= 3.14 \times 10^5$ at $N_R = 50$. On the other hand, the maximum absolute correction decreases with increasing $N_R$: MAC $= 2.95 \times 10^{-1}$ at $N_R = 10$, MAC $= 9.59 \times 10^{-2}$ at $N_R = 30$, and MAC $= 6.69 \times 10^{-2}$ at $N_R = 50$. This is because, as $N_R$ increases, the collision efficiencies overall decrease, both with and without considering the interactions between electrophoresis or gravity and diffusion. However, the decrease is less marked for the combined case than for the additive approximation. The result of this decrease is that the maximum correction factor, which is a ratio, increases as the additive approximation gives smaller and smaller predictions, whereas the maximum absolute correction, which has an upper limit of the true collision efficiency, decreases weakly as the collision efficiency is reduced. For comparision, we note that at $N_R = 30$ in the gravitational case, MCF $= 9.28 \times 10^3$ and MAC $= 2.76 \times 10^{-2}$. Both the maximum correction factor and the maximum absolute correction are larger in this case for gravity than for electrophoresis.

In all the examples shown, for values of $Q$ well below the stability boundary (the value of $Q = Q_c$, below which there would be no coagulation in the absence of Brownian motion), the error in the additive approximation is negligible, but if $Q$ is only slightly below the stability boundary, the aggregation rate is significantly larger than that predicted by either process alone. The

maximum correction factor, in particular, may be very large: for $N_R = 50$ in the gravitational case, MCF $\approx 8 \times 10^5$.

The reason the maximum correction factor is so large is simple to explain. When there is a repulsive energy barrier in the potential function, there will be a *stability boundary*, that is, a value $Q = Q_c$ below which, in the absence of Brownian motion, no aggregation will occur. The higher the energy barrier, the higher the value of $Q_c$. For a value of $Q$ just below $Q_c$, electrophoresis or gravity acting alone will not produce any aggregation whatsoever, so the additive approximation yields simply the aggregation which would occur if diffusion were present alone. However, the electrophoresis or gravity, while not causing any aggregation, effectively "climbs" most of the energy barrier, leaving only a small residual barrier to be overcome by diffusion. The aggregation due to the combination of diffusion and convection is therefore much larger than would be predicted by the additive approximation. When the repulsive barrier is smaller, it will be overcome by many particles for even fairly weak Brownian motion, so the effect of Brownian motion and electrophoresis or gravity combined will not yield a substantially larger collision efficiency than would be obtained by adding together the two (diffusive and convective) contributions.

In the results shown so far, we have kept $\kappa a$ fixed at 10. In Figs. 6 and 7 we show the effect of varying $\kappa a$ with $N_R = 30$. We observe that the maximum correction factor decreases with increasing $\kappa a$: in the gravitational case, MCF $= 1.16 \times 10^4$ at $\kappa a = 10$, while MCF $= 23.1$ at $\kappa a = 10^2$. When $\kappa a = 10^3$, there is no repulsive barrier in the potential (Type I), and the additive approximation is reasonable for all values of Pe. Though the additive approximation is not shown on the figures, the two curves are nearly indistinguishable, for $\kappa a = 10^3$.

Finally, we present one more set of data for parameters which yield a Type II potential. In this case the secondary minimum is sufficiently large and deep that its effects are noticeable in the behavior of the system with no diffusion. The parameters are $\kappa a = 10^2$, $N_R = 10$, $\nu = 0.044$, $\hat{A} = 1.25$, and $\lambda = 0.5$ and $\beta = 1$ for gravity, or $\beta = 0.5$ and $\lambda = 1$ for electrophoresis. The results are shown in Fig. 8. When there is a secondary minimum, the trajectory analysis predicts secondary aggregation for sufficiently small values of $Q$ (small enough that particles, once in the secondary minimum, cannot escape without a change in conditions). When Brownian motion is present, however, particle capture in the secondary minimum is reversible, because the secondary minimum has only finite depth, and so the particles can escape. The rest of the system behaves exactly the same as the potential discussed above, in which the secondary minimum is insignificant.

The reason that the cutoff for secondary aggregation versus $Q$ for no Brownian motion is so sharp compared to that for primary aggregation is linked to the processes causing that cutoff. As the

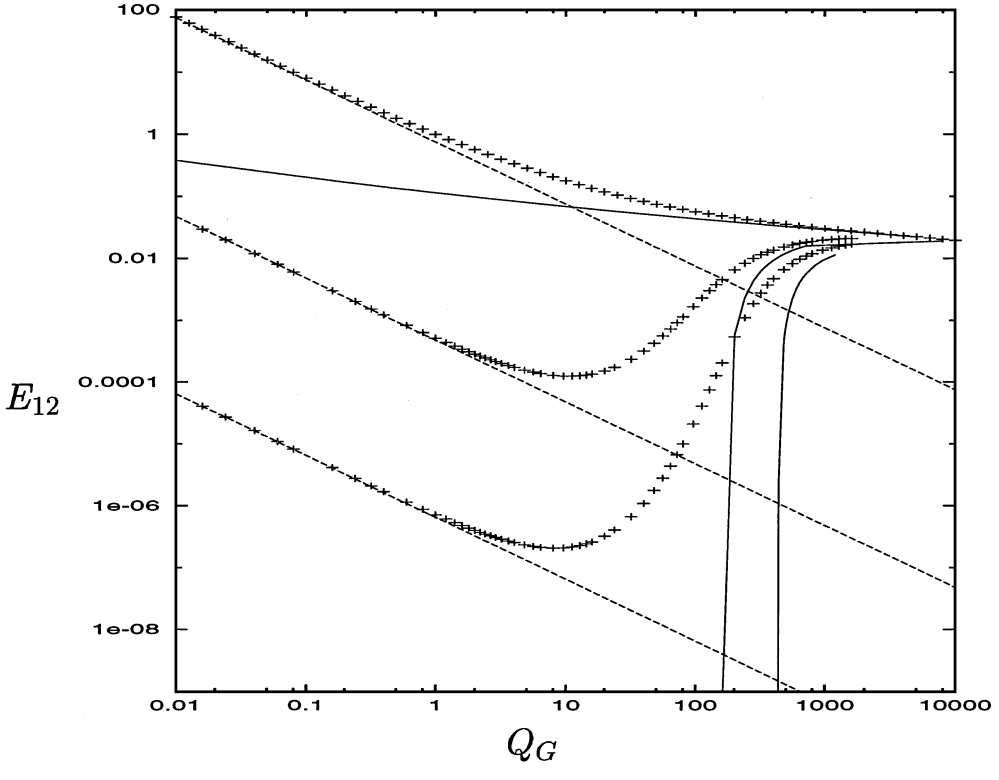


**FIG. 6.** The effect of decreasing the double-layer thickness for gravitational motion. In all cases $\lambda = 0.5$, $\nu = 0.044$, $N_R = 30$, and $\beta = 1$. Here the dotted lines correspond to only Brownian motion, the solid lines represent gravity, and the (+) represent the combined effects. The sets of plots from top to bottom correspond to $\kappa a = 10^3$, $\kappa a = 100$, and $\kappa a = 10$.

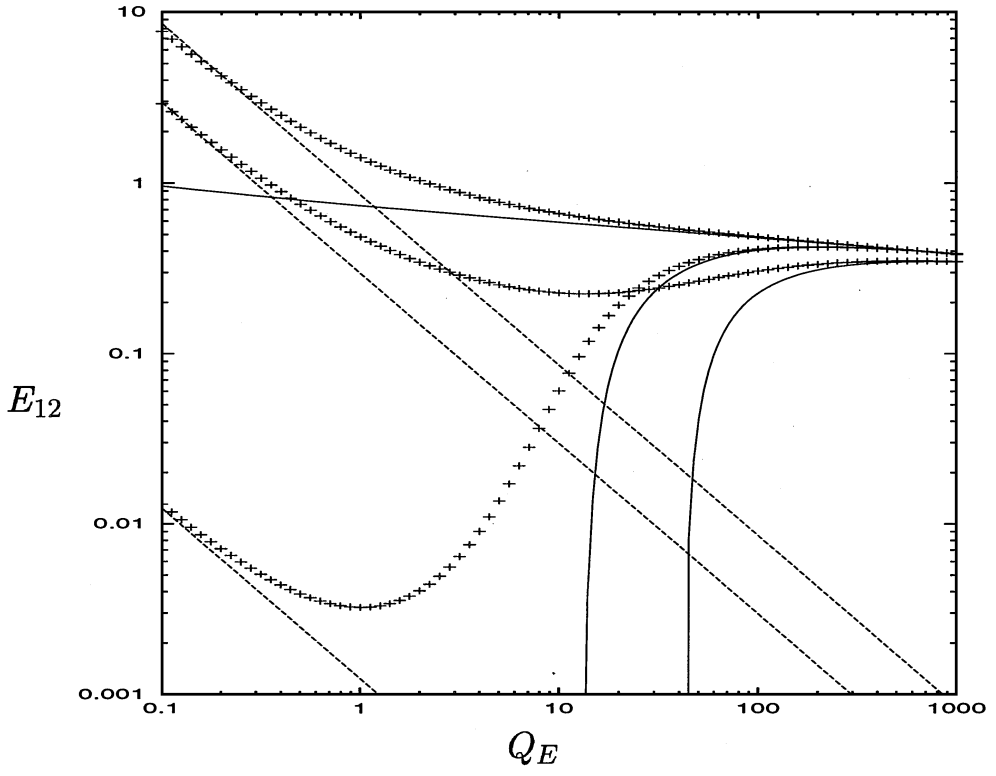


**FIG. 7.** The effects of decreasing the double-layer thickness for electrophoresis. The parameters are $N_R = 30$, $\lambda = 1$, $\beta = 0.5$, $\hat{A} = 1.25$, and $\nu = 0.044$. The solid lines represent electrophoresis only, the dashed lines Brownian motion only, and the points (+) the combination of the two effects. The values of $\kappa a$ are, reading from top to bottom, 1000, 100, and 10, respectively.

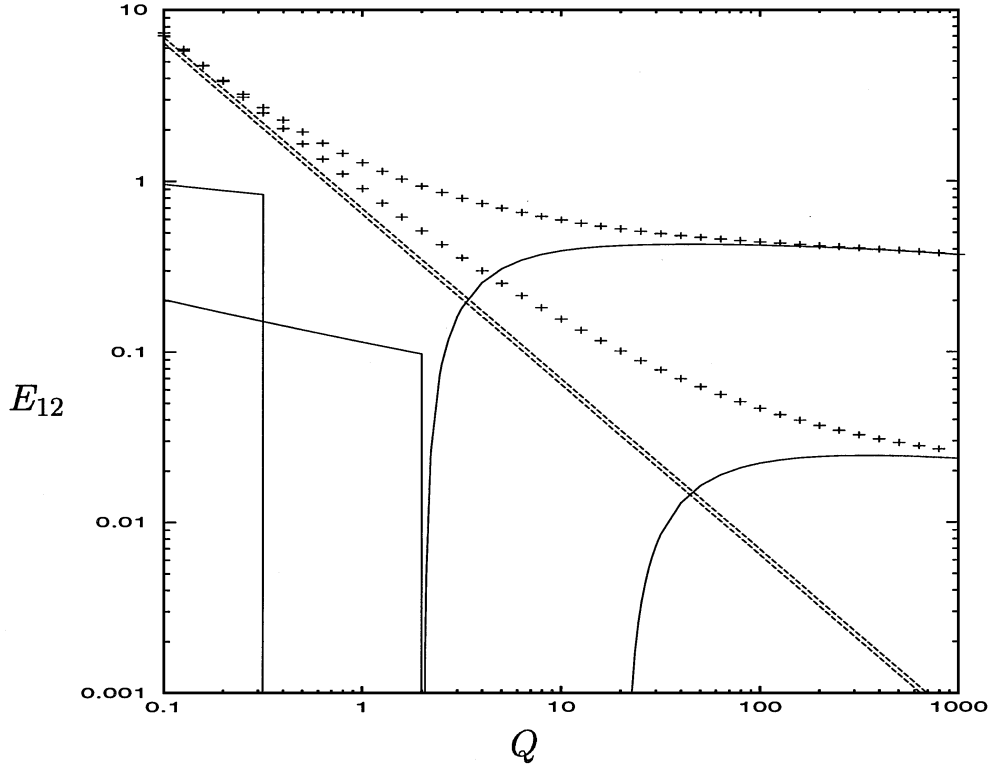


**FIG. 8.** The global system behavior for a potential which has a potential barrier and a noticeable secondary minimum. The parameters are $\kappa a = 10^2$, $N_R = 10$, $\nu = 0.044$, $\hat{A} = 1.25$ and $\lambda = 0.5$, $\beta = 1$ for gravity, and $\lambda = 1$, $\beta = 0.5$ for electrophoresis. The solid curves are for electrophoresis or gravity only; those on the right are primary aggregation and those on the left secondary aggregation. The upper curves are for electrophoresis and the lower are for gravity. The dashed lines represent aggregation due to Brownian motion alone, and the points (+) aggregation due to the combined effects of convection and diffusion.

Péclet number decreases and primary aggregation is reduced, those pairs of particles which are nearly in line for a head-on collison will continue to be able to overcome the energy barrier, while those which are further off-center are deflected and do not aggregate. This behavior can cause a small but nonzero collision efficiency for values of $Q$ slightly greater than $Q_c$. On the other hand, when secondary aggregation occurs, the trapped particles move around in the secondary minimum until they are all at the rear of the reference particle, where they stay. When the Péclet number exceeds that required to get out of the secondary minimum from the rear point and escape to infinity, all the particles will move to this point and escape, so the collision efficiency will suddenly drop to zero.

### 5.3. *Scaling Analysis*

The correction effect which we are considering is large only when there is a repulsive barrier in the potential, that is, when there is a stability boundary $Q = Q_c$ for purely convective motion, below which no aggregation occurs in the absence of diffusion. We have observed from the results in Section 5.2 that the largest correction occurs for values of $Q$ just below this boundary.

*5.3.1. Maximum correction factor (MCF).* Since the largest effect occurs when $Q$ is just less than $Q_c$, and since at that point the collision efficiency due to electrophoresis or gravity alone is zero, the maximum correction factor is simply the correction factor at $Q_c$, the ratio of our calculated collision efficiency to the Brownian limit $C/\mathrm{Pe} = C/\hat{A}Q$. All that remains, then, is to predict the collision efficiency $E_{12}$. We have considered two alternative approximations.

For $Q_c - Q \ll 1$ the electrophoresis or gravity has almost enough energy to overcome the potential energy barrier, so we may consider the system as approximately equivalent to one with Brownian motion acting alone, and no repulsive barrier in the potential. We model this system by using the same parameters as the original system, but "turning off" the electrostatic force. Then the Brownian collision efficiency prediction is given by $C'/\hat{A}Q_c$, where $C'$ is calculated from [14] using the attractive potential function.

Alternatively, if the cutoff between no aggregation and primary aggregation for no Brownian motion were very sharp, then the collision efficiency for $Q - Q_c \ll 1$ would be approximately equal to that for no Brownian motion at $Q = Q_c$ with the electrostatic force "turned off" This estimate is provided numerically here, by a trajectory analysis, or it could be found using the asymptotic results [17] of Davis (8) for $Q \gg 1$. We refer to it as the convective method of approximation.

The results of the above estimates for the maximum correction factor (for all sets of parameter values presented in the preceding sections, except those in which there is no repulsive energy barrier) are plotted in Fig. 9. We have plotted our predicted maximum correction factors against the computed value. It is seen that the first (diffusive) estimation method almost always

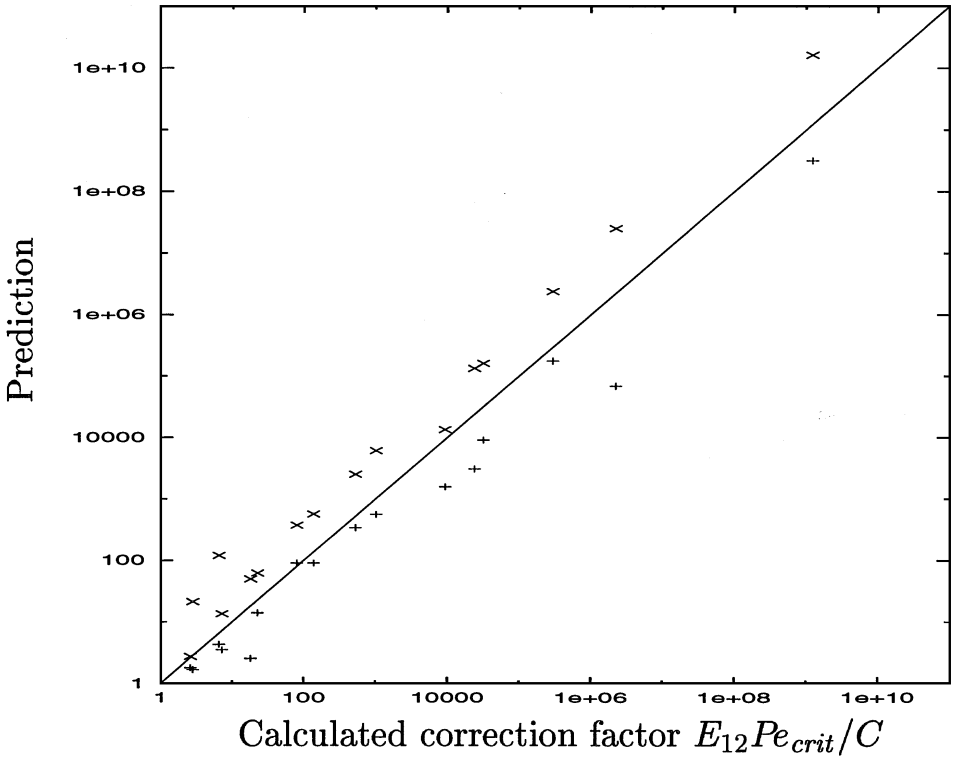


**FIG. 9.** The predicted maximum correction factors from the diffusive (+) and convective (×) methods are plotted against our calculated maximum correction factor.

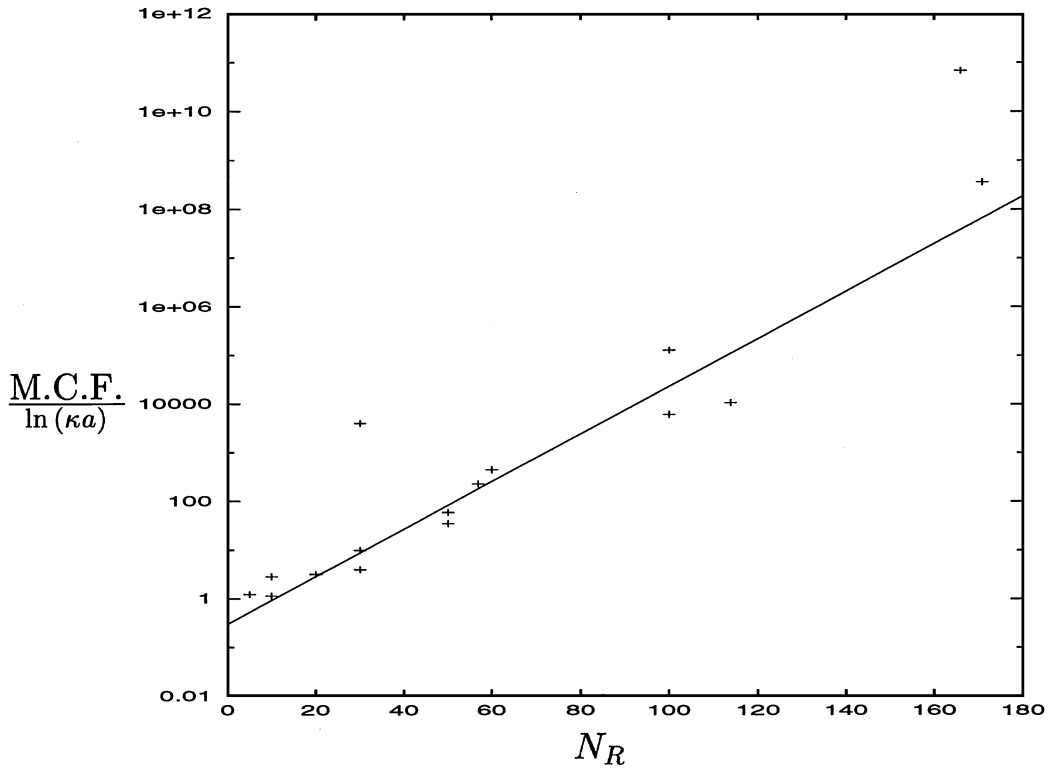


**FIG. 10.** The maximum correction factor (scaled by $\ln(\kappa a)$) plotted against $N_{\mathrm{R}}$, together with the exponential scaling predicted by Eq. [31]. The points (+) are the numerical values, while the solid line is the scaling analysis prediction, with a best fit of $0.3\exp(0.09\hat{A}N_{\mathrm{R}})$.

underpredicts the collision efficiency, while the second (convective) method systematically overpredicts it. We can therefore present rough bounds on the collision efficiency. However, the maximum absolute value of the correction (i.e., calculated collision efficiency minus additive approximation, as opposed to collision efficiency divided by additive approximation) is not very well predicted by either of these methods.

The value of $C'$, the low-Péclet-number integral, in all these cases is between 0.85 and 1.4, so the maximum correction factor scales approximately as $C^{-1}$. As a rough guide, this gives

$$\begin{aligned}\mathrm{MCF} &\propto C^{-1} \\ &= \int_2^{\infty} \frac{\exp(\hat{A}\phi(s))}{s^2 G(s)}\,\mathrm{d}s \\ &\propto \int_{2+(\kappa a)^{-1}}^{\infty} \frac{\exp(\hat{A}\phi_{\max})}{s^2(s-2)}\,\mathrm{d}s \\ &\propto \exp(\hat{A}\phi_{\max})\ln(\kappa a) \\ &\propto \exp(A_0\hat{A}N_{\mathrm{R}})\ln(\kappa a). \qquad [31]\end{aligned}$$

In Fig. 10 we plot the true value of the maximum correction factor divided by $\ln(\kappa a)$ against $N_{\mathrm{R}}$, and show the curve given by the above expression with $A_0 = 0.09$, for all the results we have shown in other plots in this paper. Since the value of $C$ is easy to calculate (a simple numerical quadrature), in Table 2 we tabulate values of $C$ against some of our numerical parameters.

*5.3.2. Maximum absolute correction (MAC).* We consider the dependence of the maximum absolute correction on the

**TABLE 2**
**Values of the Brownian Motion Aggregation Constant $C$ for Different Values of the Parameters $\kappa a$ and $N_{\mathrm{R}}$**

| $\kappa a$ | $N_{\mathrm{R}}$ | $C$ | $\kappa a$ | $N_{\mathrm{R}}$ | $C$ |
|---|---|---|---|---|---|
| 5 | 5 | $3.602\times10^{-1}$ | 100 | 5 | $8.413\times10^{-1}$ |
| 5 | 10 | $8.723\times10^{-2}$ | 100 | 10 | $7.996\times10^{-1}$ |
| 5 | 50 | $2.306\times10^{-8}$ | 100 | 50 | $6.292\times10^{-3}$ |
| 5 | 100 | $4.338\times10^{-17}$ | 100 | 100 | $1.260\times10^{-8}$ |
| 5 | 500 | $3.077\times10^{-89}$ | 100 | 500 | $1.091\times10^{-66}$ |
| 10 | 5 | $4.719\times10^{-1}$ | 500 | 5 | $8.675\times10^{-1}$ |
| 10 | 10 | $1.521\times10^{-1}$ | 500 | 10 | $8.674\times10^{-1}$ |
| 10 | 50 | $1.027\times10^{-7}$ | 500 | 50 | $8.665\times10^{-1}$ |
| 10 | 100 | $4.039\times10^{-16}$ | 500 | 100 | $8.640\times10^{-1}$ |
| 10 | 500 | $8.851\times10^{-87}$ | 500 | 500 | $1.770\times10^{-30}$ |
| 50 | 5 | $7.735\times10^{-1}$ | 1000 | 5 | $8.676\times10^{-1}$ |
| 50 | 10 | $6.094\times10^{-1}$ | 1000 | 10 | $8.676\times10^{-1}$ |
| 50 | 50 | $6.306\times10^{-5}$ | 1000 | 50 | $8.675\times10^{-1}$ |
| 50 | 100 | $7.610\times10^{-12}$ | 1000 | 100 | $8.675\times10^{-1}$ |
| 50 | 500 | $1.698\times10^{-75}$ | 1000 | 500 | $1.739\times10^{-6}$ |

*Note.* The other parameters (which have a much less dramatic effect on the values of $C$) are fixed at $\lambda = \beta = 1$, $\nu = 0.044$, and $\hat{A} = 1.25$.

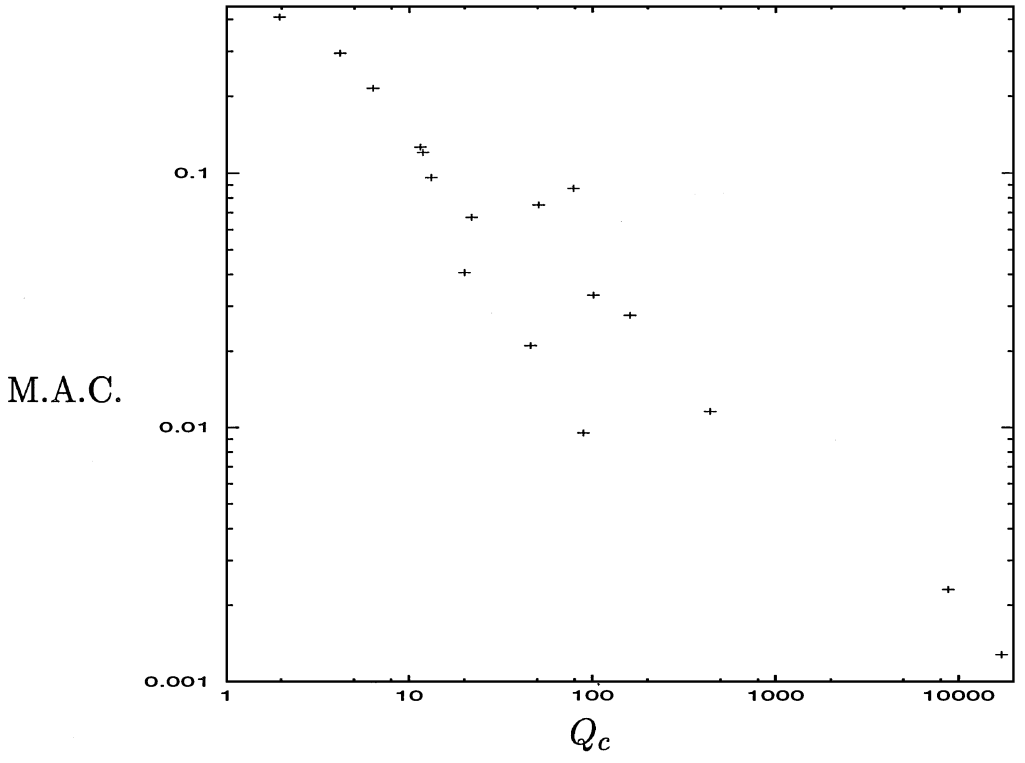


**FIG. 11.** The maximum absolute correction plotted against $Q_c$. The points are all the electrophoretic results shown elsewhere in the paper.

value of the stability boundary $Q_c$. If the boundary is very high, ($Q_c \gg 1$), then it is an indicator of a large energy barrier in the interparticle potential. The collision efficiencies will all be small (no matter which method is used to calculate them), so the maximum absolute correction cannot be very large. On the other hand, if the boundary is very low, then the pure Brownian contribution just below the barrier, $E_{12}^{\mathrm{B.M.}} = C/\hat{A}Q_c$, will be large. Although this result might suggest that the Brownian contribution will be close to the true collision efficiency, in fact this argument only applies to the maximum correction factor. A change in the collision efficiency of a few percent (which will be irrelevant physically when aggregation is fast) can lead to a large maximum absolute correction. Therefore, we predict that MAC will decrease with increasing $Q_c$.

In Fig. 11, the maximum absolute correction is plotted against $Q_c$ for all the results we have shown for electrophoresis. It is seen that the maximum absolute correction does indeed decrease weakly with increasing $Q_c$. The values of $Q_c$ are determined using a trajectory analysis, in which successively lower values of $Q$ are used until the collision efficiency due to electrophoresis or gravity alone becomes zero.

*5.3.3. Dangerous parameter range.* In this section we consider the behavior of the maximum absolute correction and maximum correction factor with a varying dimensionless height of the potential barrier. As (broadly speaking) MAC decreases and MCF increases with barrier height, we can identify an approximate parameter range in which the additive approximation may give results which are significantly in error.

For the maximum absolute correction, we choose to impose the restriction that, for the difference to be significant, the maximum absolute correction must be at least 0.02. This choice leads to the condition $\phi_{\max} \lesssim 6$. For the maximum correction factor, we use the restriction that the maximum correction factor must be at least 5 for the maximum correction to be considered significant. This choice, in turn, leads to the condition $\phi_{\max} \gtrsim 0.5$. Therefore we conclude that the additive approximation should not be trusted to give results which are qualitatively correct if $0.5 \lesssim \phi_{\max} \lesssim 6$. If the repulsive barrier is lower than this range, then the synergistic effects of Brownian and electrophoretic or gravitational motion increase the collision rate by only a few-fold, or less, over that from Brownian and convective motion acting independently. On the other hand, if the repulsive barrier is higher than this range, then the collision rates remain very low, even with a large maximum correction factor.

### 5.4. Physical Examples

*5.4.1. Electrophoresis.* In order to illustrate the physical results of our investigation, we consider a system in which there are regimes of both weak and moderate Brownian motion corresponding to small and larger particles. We fix the physical parameters at $\kappa^{-1} = 0.1\,\mu$m, which corrresponds (20) to a room-temperature ($kT = 4 \times 10^{-21}$ J) solution of 10 $\mu$M NaCl, $\epsilon = 7.115 \times 10^{-10}$ JV$^{-2}$ m$^{-1}$, $\lambda_L = 0.1\,\mu$m, and $A = 5 \times 10^{-21}$ J.

We consider two different $\zeta$-potentials ($\zeta_i = 10$ mV or 20 mV). Since the mobilities do not depend on the parameter

$\beta$, and both the electrostatic force and the far-field velocity $V_{12}^{(E;0)}$ are symmetrical in $\beta$ and $\beta^{-1}$, we may set $\beta = 0.5$ for all the interactions (regardless of whether our formulation leads to $\beta = 0.5$ or $\beta = 2$).

The dimensionless parameters become

$$\begin{aligned} \beta &= 0.5 \qquad \kappa a = 10a \\ \hat{A} &= 1.25 \qquad N_{\mathrm{R}} = 28.46a \\ \nu &= 0.1/a \quad Q_{\mathrm{E}} = 0.5364 E a^2 \lambda/(1+\lambda)^2, \end{aligned}$$

where $a$ is in micrometers and $E$ has units of $\mathrm{Vmm}^{-1}$. We note that only pairs of particles with different $\zeta$-potentials can aggregate in electrophoresis, because two particles with the same $\zeta$-potential have the same electrophoretic velocity, so their relative velocity (and ability to collide) is zero. We note that, for $a = O(1\,\mu\mathrm{m})$, the interparticle potential is of Type II; i.e., it has a repulsive energy barrier.

The results of performing the computations for each pairwise interaction are shown in Fig. 12, when the smaller particles have 1-$\mu$m radius and the larger have 3-$\mu$m radius. As we would expect, for weak electric fields $E \lesssim 10\ \mathrm{Vmm}^{-1}$, the aggregation is largely driven by Brownian motion and the collision efficiency is similar to that predicted from Brownian motion acting alone. For strong electric fields $E \gtrsim 100\ \mathrm{Vmm}^{-1}$, the aggregation is nearly independent of the presence of Brownian motion, and a trajectory analysis gives a good qualitative picture of the collision efficiency. However, it is at moderate electric fields, for which a trajectory analysis predicts a stable suspension, that the most dramatic effect of Brownian motion is seen. When $10\ \mathrm{Vmm}^{-1} < E < 100\ \mathrm{Vmm}^{-1}$, the maximum correction factors for all three combinations of particles are between $10^3$ and $10^8$. The maximum absolute corrections are all in the range 0.03–0.13, with the case of two small particles, in which MAC = 0.12, showing an increase from a low predicted collision efficiency of $E_{12} = 2.3 \times 10^{-4}$ to a much larger value of $E_{12} = 0.12$.

*5.4.2. Gravity.* A study accomplished by Han *et al.* (21) calculated the amount of Brownian coagulation in rain, rivers and lakes, estuaries, and seas under realistic parameter values. The paper presented a figure of surface potential as a function of ionic strength, for different particle size ratios, $\lambda$. For each value of $\lambda$ they identified parameter regimes in which substantial coagulation would occur.

We have used their parameters to choose suitable parameters for rain and river water and have calculated collision efficiencies for Brownian motion and gravity acting separately, and for Brownian motion plus gravity acting together. In these

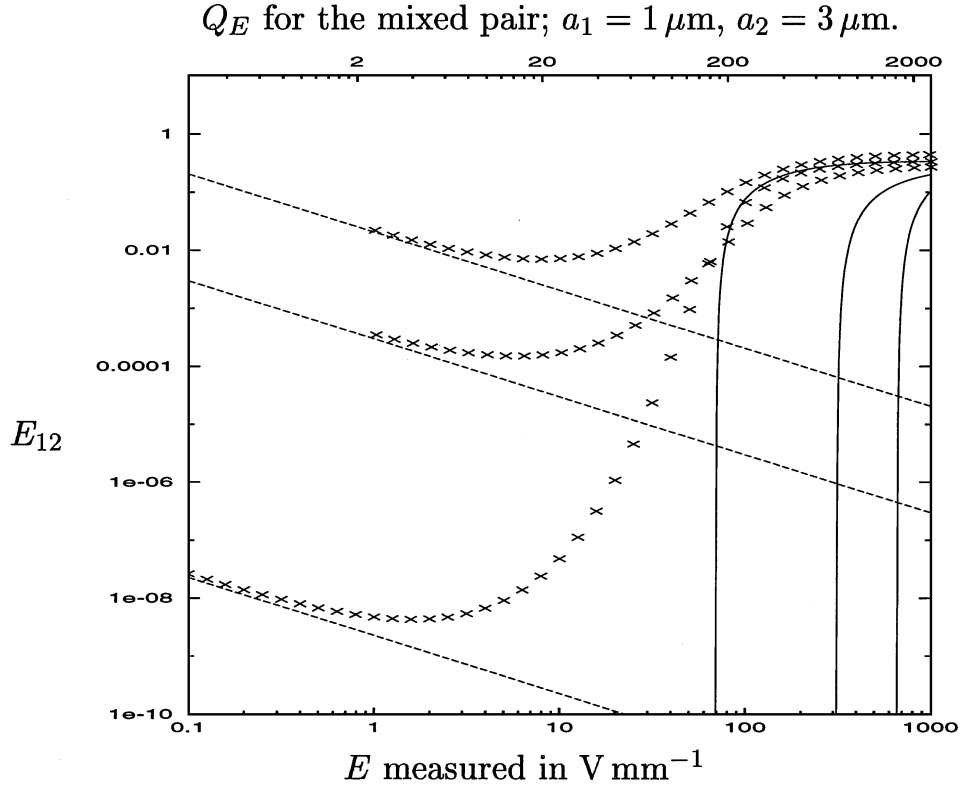


**FIG. 12.** Collision efficiencies for different pairs of particles, plotted against the electric field $E$. On the top axis are shown the values of $Q_{\mathrm{E}}$ for the small–large interactions. The lines represent, reading from top to bottom at the left-hand side, small–small, small–large, and large–large collisions, respectively. The small and large particle radii are 1 and 3 $\mu$m, respectively, and each interaction is between a pair of particles having charges 10 and 20 mV. The collision efficiencies which would result from Brownian motion alone are given by the dashed lines, and those for electrophoretic motion alone by the solid curves. The points ($\times$) show the actual collision efficiency.

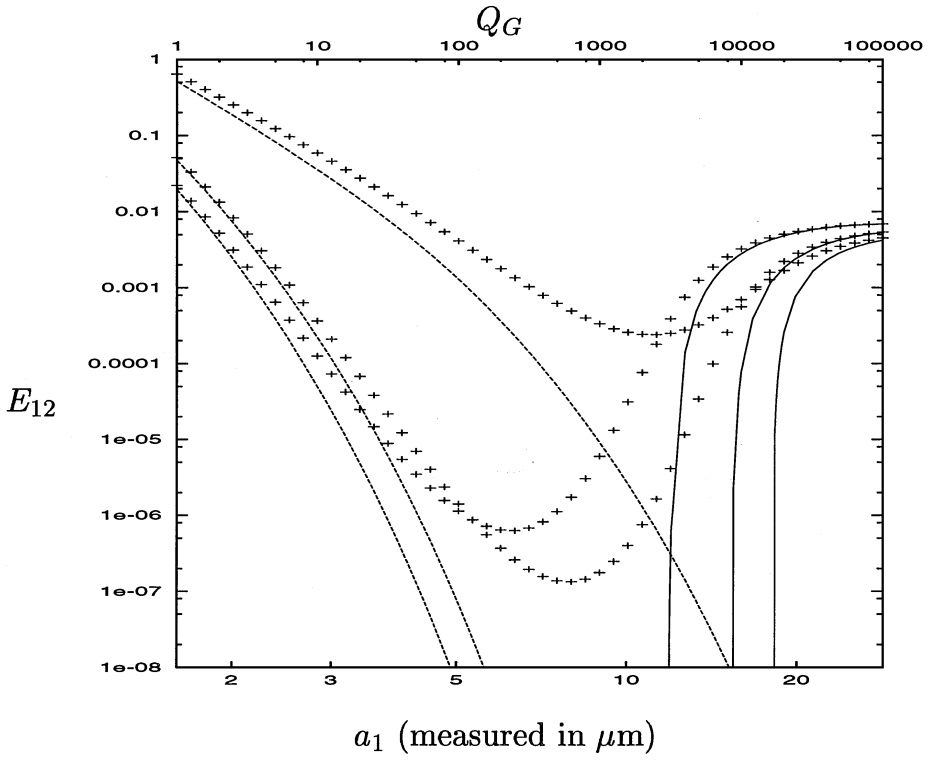


**FIG. 13.** Collision efficiencies predicted for realistic parameter values in gravitational sedimentation. The collision efficiency is plotted against the larger radius, $a_1$ $\mu$m, on the lower abscissa, and $Q_{12}$, along the upper abscissa. The dashed curves represent Brownian motion and, from top to bottom, correspond to $\kappa = 50$, 10, and 5 $\mu$m$^{-1}$, or ionic strengths of $\approx$200, 10, and 5 $\mu$M. The solid lines on the right represent collisions due to sedimentation only, and from right to left correspond to $\kappa = 5$, 10, and 50 $\mu$m$^{-1}$. The points (+) represent the combined effects. Note the crossings of these curves.

calculations we allow the average radius $a$ to vary. Due to the limited amount of numerical parameters given, we have also chosen typical hydrosol parameters (20).

Figure 13 is a plot of the collision efficiencies as a function of $Q_G$ and $a$, which we have calculated for the dimensionless parameters, which are expressed as a function of $a$ in micrometers, given below:

$$\begin{aligned} \hat{A} &= 1.25 \quad & N_R &= 14.23a \\ \lambda &= 0.5 \quad & \kappa a &= 5a, 10a, 50a \\ \beta &= 1 \quad & \nu &= 0.1/a. \end{aligned}$$

These parameters correspond to a 5-, 10-, or 200-$\mu$M solution of a 1 : 1 electrolyte with

$$\begin{aligned} A &= 5 \times 10^{-21}\ \text{J} \\ \zeta_i &= 10\ \text{mV} \\ \lambda_L &= 0.1\mu\text{m} \\ \epsilon &= 7.115 \times 10^{-10}\ \text{JV}^{-2}\,\text{m}^{-1}. \end{aligned}$$

Unlike the graphs presented previously, the collision efficiency in Fig. 13 due to thermal motion is a curve, not a straight line. Here $C$ is a function of the dimensionless variable $\nu$, which is calculated with $a$. Therefore, each $a$ value corresponds to a different $C$, producing the curved plot.

The collision efficiency curves for $\kappa = 5\,\mu\text{m}^{-1}$ and $\kappa = 10\,\mu\text{m}^{-1}$ cross at a value of $a \approx 5\,\mu$m. This crossing is indicative of two competing effects. The area to the left of the crossing is dominated by thermal aggregation, and as expected, the particles with the thicker double layer $\kappa = 5\,\mu\text{m}^{-1}$ will aggregate less than those with the thinner double layer $\kappa = 10\,\mu\text{m}^{-1}$, because the energy potential barrier is weaker in the former case. However, the collisions predicted from sedimentation to the right of the crossing show an opposite trend, with collision efficiencies higher for $\kappa = 5\,\mu\text{m}^{-1}$ than for $\kappa = 10\,\mu\text{m}^{-1}$. This result is contrary to the Brownian result, but it may be explained by consideration of the mechanism for aggregation. When the crossing occurs, the Péclet number is larger (around $10^4$), so aggregation is largerly driven by sedimentation. At these Péclet numbers, enough energy is supplied by the relative motion due to sedimentation to cause many particles to overcome the energy barrier. However, the incoming particle is swept around the side of the slower-moving particle very quickly, before it can "fall" deep into the primary minimum in the potential. When it reaches the rear of the slower particle, there may be enough energy remaining to pull it back out of the minimum and allow it to escape to infinity. A higher potential energy barrier will reduce the number of particles escaping from the primary minimum, and hence we see that at high Péclet numbers, a larger energy barrier actually causes a higher collision

efficiency. When $\kappa = 50\,\mu$m, the potential is entirely attractive and has the lowest of the three collision efficiencies at high values of $Q$.

The maximum correction factor increases as $\kappa$ increases from 5 to $10\,\mu\text{m}^{-1}$, due to the effects outlined above, and then it decreases from $\kappa = 10\,\mu\text{m}^{-1}$ to $50\,\mu\text{m}^{-1}$. With an increase in the repulsive barrier, we observe a decrease in $Q_c$, where sedimentation-based flocculation begins to have a significant effect. Therefore, in the presence of a repulsive barrier, including sedimentation-based aggregation as well as thermal collisions is critical to the formulation of an accurate picture of suspension stability.

We predict a moderate value of the collision efficiency for virtually all values of Pe, using our specified parameter values. Therefore, we observe the importance of including both thermal and gravitational motion, and utilizing the correct method for determination of the collision efficiency for similar studies.

### 5.5. *Comparison between Gravity and Electrophoresis*

In this section, we match parameters as far as possible between the two situations, in order to compare the magnitude of the effect of combined Brownian motion and convection (relative to the simple sum of the two) between the two driving forces. The common parameters we have chosen are

$$\lambda = 0.5 \qquad \kappa a = 10$$
$$\beta = 0.5 \qquad N_{\text{R}} = 25$$
$$\hat{A} = 1.25 \qquad \nu = 0.044,$$

and we plot the collision efficiencies against $Q_{(\text{G,E})}$. Physically, $Q$ may be varied in the electrophoretic case by varying the electric field $E$, and in the gravitational case by varying the density difference $\Delta\rho$ between the particles and the ambient fluid. Although it is more usual to consider a Péclet number which varies with particle size, we find that for direct comparision between the two cases it is simpler to fix the particle size. We note that the pure Brownian limit $C/\text{Pe}$ is identical in the two cases, as it depends only on the form of the interparticle potential.

The results from this calculation are shown in Fig. 14. The absolute collision efficiencies are larger for electrophoresis than for gravity, as discussed previously (9). In the gravitational case, MCF = 80.5 and MAC = $9.49 \times 10^{-3}$, and for electrophoresis, MCF = 137 and MAC = 0.127. We note that, unlike the data presented in Figs. 4 and 5, in this case both corrections are larger for the electrophoresis case than for gravity. We conclude that the effects are not systematically larger in either system.

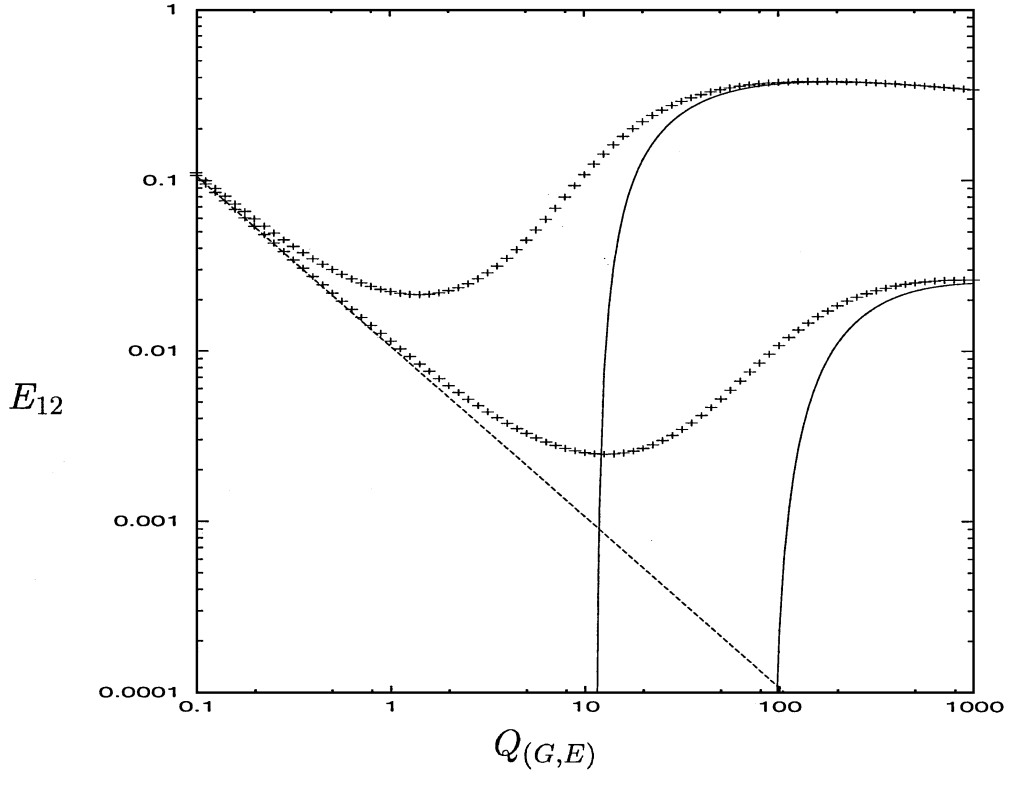


**FIG. 14.** Plot of the collision efficiency $E_{12}$ against driving force $Q_{\text{G}}$ or $Q_{\text{E}}$, for the parameters specified in Section 5.5. The dashed line is the pure Brownian limit, and the solid lines on the right are the limit of no Brownian motion, calculated by trajectory analysis. The points (+) are for convection and diffusion combined. The upper curve is for electrophoresis and the lower curve is for gravity.

The reason that there is any difference between gravity and electrophoresis is contained in the mobility functions. At small separations under electrophoresis, as explained by Wang *et al*. (10), there is electrically driven convection in the electrical double layer, which facilitates approach of the particles. Therefore the electrophoretic mobilities are much larger than those for gravity at close separations.

## 6. CONCLUSIONS

The collision efficiency of solid particles which are simultaneously affected by gravity or electrophoresis and Brownian motion was considered, taking into account the effects of retarded van der Waals, electrostatic, and hydrodynamic forces. The calculations were performed by numerical solution of the quasi-steady Fokker–Planck equation for the pair distribution function. These collision efficiencies were compared to an "additive approximation" calculated by summing the collision efficiencies induced by Brownian motion and electrophoresis or gravity acting independently.

The two methods of calculating the collision efficiency can be very different when electrophoresis or gravity acting alone is only slightly too weak to allow incoming particles to overcome a large energy barrier in the interparticle potential. Brownian motion then permits large numbers of particles to overcome the remaining energy barrier and aggregate.

The maximum correction factor, which is the factor by which the collision efficiency is increased when the full problem is considered, is larger for larger energy barriers in the interparticle potential. The maximum absolute correction, on the other hand, is small for very large energy barriers.

For the correction to the aggregation to be physically significant, both the maximum correction factor and the maximum absolute correction need to be of moderate size, which can occur when the interpaticle potential has a maximum value between $0.5A$ and $6A$ (with $A$ as the Hamaker constant). We conclude that, in this regime, the additive approximation is not valid, and the effects of electrophoresis or gravity and diffusion acting simultaneously must be considered to obtain an accurate physical model.

## ACKNOWLEDGMENTS

This work was supported by NASA Grant NAG3-1850 and NSF Grant CTS-9416702. The authors thank Dr. Alexander Zinchenko and Dr. Shulin Zeng for making available their codes.

## REFERENCES

1. von Smoluchowski, M., *Bull. Int. Acad. Sci. Cracovie* **8,** 182 (1903).
2. Russel, W. B., Saville, D. A., and Schowalter, W. R., "Colloidal Dispersions." Cambridge University Press, Cambridge, UK, 1989.
3. Derjaguin, B., and Landau, L., *Acta Physicochim.* **14,** 633 (1941).
4. Verwey, E., and Overbeek, J., "Theory of the Stability of Lyophobic Colloids." Elsevier, Amsterdam, New York, 1948.
5. Hamaker, H. C., *Physica* **4,** 1058 (1937).
6. Spielman, L. A., *J. Colloid Interface Sci.* **33,** 562 (1970).
7. Melik, D. H., and Fogler, H. S., *J. Colloid Interface Sci*. **101,** 72 (1984).
8. Davis, R. H., *J. Fluid Mech*. **145,** 179 (1984).
9. Nichols, S. C., Loewenberg, M., and Davis, R. H., *J. Colloid Interface Sci*. **176,** 342 (1995).
10. Wang, H., Zeng, S., Loewenberg, M., and Davis, R. H., *J. Colloid Interface Sci*. **187,** 213 (1997).
11. Zeng, S., Zinchenko, A. Z., and Davis, R. H., *J. Colloid Interface Sci*. **209,** 282 (1999).
12. Zinchenko, A. Z., and Davis, R. H., *J. Fluid Mech*. **280,** 119 (1994).
13. Zinchenko, A. Z., and Davis, R. H., *Phys. Fluids* **7,** 2310 (1995).
14. Batchelor, G. K., *J. Fluid Mech*. **74,** 1 (1976).
15. Zhang, X., and Davis, R. H. *J. Fluid Mech*. **230,** 479 (1991).
16. Elimelech, M., Gregory, J., Jia, X., and Williams, R., "Particle Deposition and Aggregation: Measurement, Modeling and Simulation." Butterworth–Heinemann, Stoneham, MA/London, 1995.
17. Ho, N. F. H., and Higuchi, W. I., *J. Pharm. Sci*. **57,** 436 (1968).
18. Dukhin, S. S., and Lyklema, J., *Colloid J. USSR* **53,** 402 (1991).
19. Hogg, R., Healy, T. W., and Fuerstenau, D. W. *Faraday Soc. Trans*. **62,** 1638 (1966).
20. Hiemenz, P. C., "Principles of Colloid and Surface Chemistry." Dekker, New York, 1977.
21. Han, M., Lee, H., Lawler, D. L., and Choi, S., *Water Sci. Technol*. **36**(4), 69 (1997).